A paleogeodetic record of variable interseismic rates and megathrust coupling at Simeulue Island, Sumatra

Tsang, Louisa Lok Hang; Meltzner, Aron Jeffrey; Hill, Emma Mary; Freymueller, Jeffrey T.; Sieh, Kerry

2015

Tsang, L. L. H., Meltzner, A. J., Hill, E. M., Freymueller, J. T., & Sieh, K. (2015). A paleogeodetic record of variable interseismic rates and megathrust coupling at Simeulue Island, Sumatra. Geophysical Research Letters, 42(24), 10585-10594.

https://hdl.handle.net/10356/81768

https://doi.org/10.1002/2015GL066366

AGU PUBLICATIONS

Geophysical Research Letters

RESEARCH LETTER
10.1002/2015GL066366

Key Points:
- An ~1100 year paleogeodetic record reveals time-varying interseismic deformation rates
- Modeling suggests that changes in fault coupling over decades to centuries can explain these rates
- GPS-derived coupling maps represent only a snapshot of fault conditions that can change with time

Supporting Information:
- Text S1
- Text S2
- Table S1
- Table S2
- Table S3
- Table S4

Correspondence to:
E. M. Hill,
ehill@ntu.edu.sg

Citation:
Tsang, L. L. H., A. J. Meltzner, E. M. Hill, J. T. Freymueller, and K. Sieh (2015), A paleogeodetic record of variable interseismic rates and megathrust coupling at Simeulue Island, Sumatra, *Geophys. Res. Lett.*, *42*, doi:10.1002/2015GL066366.

Received 5 OCT 2015
Accepted 19 NOV 2015
Accepted article online 24 NOV 2015

A paleogeodetic record of variable interseismic rates and megathrust coupling at Simeulue Island, Sumatra

Louisa L. H. Tsang[1,2], Aron J. Meltzner[1], Emma M. Hill[1,2], Jeffrey T. Freymueller[3], and Kerry Sieh[1,2]

[1]Earth Observatory of Singapore, Nanyang Technological University, Singapore, [2]Asian School of the Environment, Nanyang Technological University, Singapore, [3]Geophysical Institute, University of Alaska Fairbanks, Fairbanks, Alaska, USA

Abstract An ~1100 year long paleogeodetic record of land-height change along the Simeulue section of the Sumatran subduction zone reveals significant variations in vertical motion rates. From an ~267 year long record, we develop models to explain rate variations in the decades before the 1861, 2004, and 2005 great earthquakes. The record shows that rates accelerated by a factor of 4 to 10 in the decades before the 1861 earthquake; one plausible explanation is a significant increase in the depth of interseismic coupling on the Sunda megathrust under Simeulue. Despite similarity of the 1861 and 2005 coseismic rupture patterns, the pattern of coupling during the decades before the two earthquakes may have been different. Most GPS observations of interseismic deformation at subduction zones span only a decade or two; our results highlight the need to treat GPS-derived coupling maps as only a snapshot of fault conditions that are temporally variable.

1. Introduction

Fault coupling represents the pattern of interseismic strain accumulation on a fault, expressed as the ratio of the slip rate deficit during the interseismic period to the plate convergence rate. Highly coupled patches are regions of the fault that can potentially release a large portion of strain seismically in large earthquakes. Therefore, assessing the location and size of future earthquakes along active faults requires characterizing the patchwork quilt of interseismic fault coupling patterns. Maps of interseismic fault coupling are usually derived from GPS data spanning one or two decades and are useful for identifying rupture segments based on matching interseismic coupling patterns with past earthquake rupture areas [e.g., *Kaneko et al.*, 2010; *Miura et al.*, 2004; *Moreno et al.*, 2010; *Loveless and Meade*, 2011; *Metois et al.*, 2012], identifying potential rupture barriers [e.g., *Prawirodirdjo et al.*, 2010; *Chlieh et al.*, 2008] and understanding various stages of the seismic cycle on adjacent fault segments [e.g., *Moreno et al.*, 2011; *Freymueller et al.*, 2000]. However, some researchers have found little correlation between areas of fault coupling and earthquake rupture, and advocate for augmenting GPS-inferred coupling maps with multicycle slip histories along megathrusts [e.g., *Lorito et al.*, 2011; *Romano et al.*, 2012; *Nalbant et al.*, 2013; *Wesson et al.*, 2015; *Thirumalai et al.*, 2015]. This advocacy is well justified in light of what we now understand about the host of tectonic processes that occur on megathrusts during the interseismic period of the seismic cycle. Transient processes such as slow slip events, afterslip, and viscoelastic relaxation of the mantle (that can potentially extend over time periods beyond a seismic cycle) can alter deformation patterns and stress states on megathrusts over long time periods [e.g., *Suito and Freymueller*, 2009; *Paul et al.*, 2012; *Meade and Loveless*, 2009; *Fu and Freymueller*, 2013; *Tsang et al.*, 2015] and thus complicate the interpretation of interseismic deformation.

Furthermore, long-duration geodetic records in the Alaska, Chile, Japan, and Sumatra subduction zones reveal that strain may not accumulate linearly during the interseismic period [*Nishimura et al.*, 2004; *Prawirodirdjo et al.*, 2010; *Philibosian et al.*, 2014; *Li et al.*, 2014; *Meltzner et al.*, 2015; *Wesson et al.*, 2015]. Such spatiotemporal variability needs to be characterized holistically, along with the tectonic processes that control that variability, if we are to improve assessment of seismic hazard along megathrusts. To achieve this objective, we need to study geodetic records spanning several seismic cycles. In contrast, most GPS coupling maps represent only a snapshot of the interseismic period.

Along the Sumatran subduction zone, *Meltzner et al.* [2010, 2012, 2015] reconstructed interseismic vertical deformation histories by analyzing coral microatolls from multiple sites located across Simeulue Island,

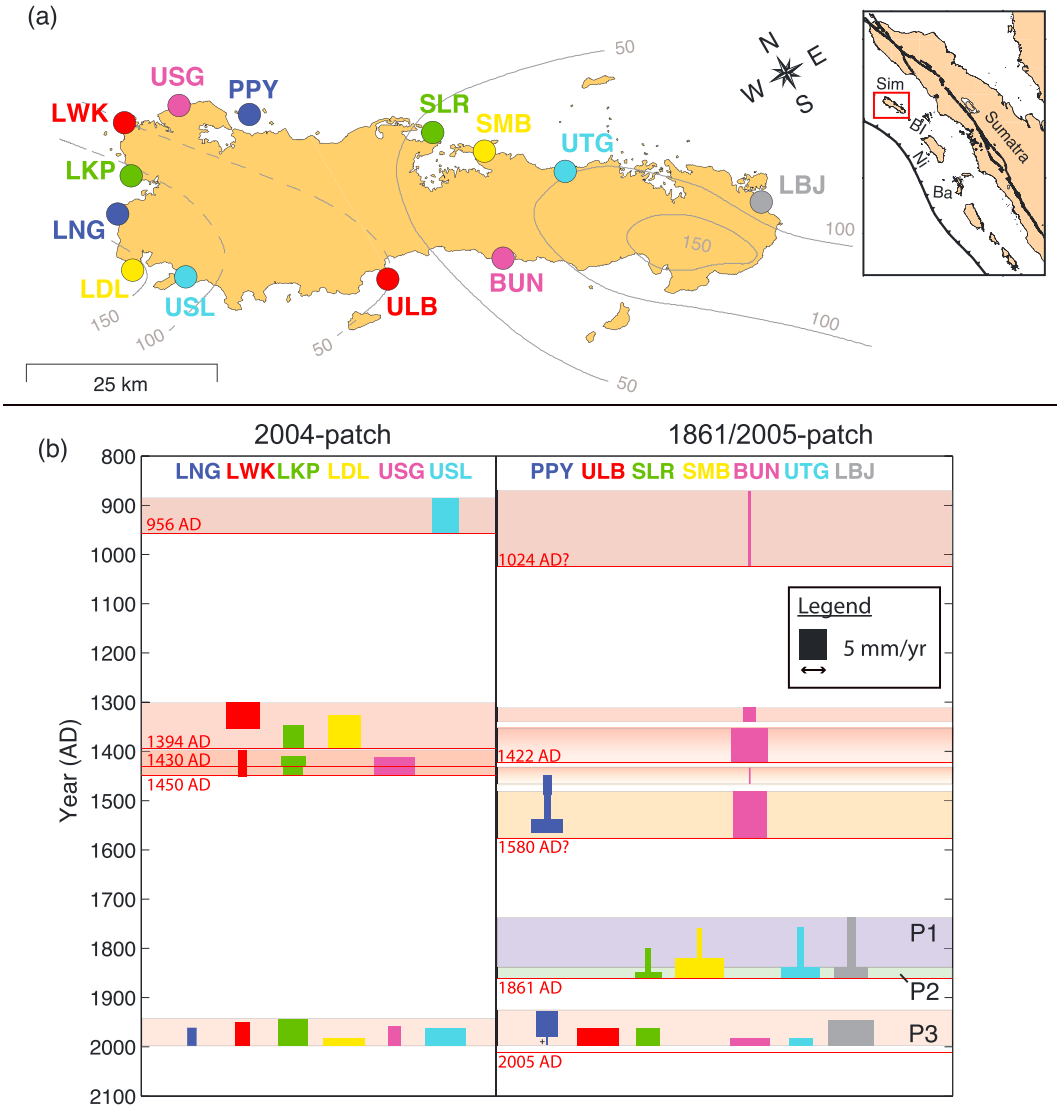

Figure 1. (a) Simeulue Island is located offshore of north Sumatra (inset). Sim: Simeulue, Bl: Banyak Islands, Ni: Nias, and Ba: Batu Islands. *Meltzner et al.* [2010, 2012, 2015] reconstructed interseismic uplift histories from coral microatolls sampled at 13 sites across Simeulue Island (main). Contours indicate the coseismic uplift (in cm) during the 2004 M_w 9.2 Sumatra-Andaman earthquake (dashed grey, from *Meltzner et al.* [2012]) and 2005 M_w 8.6 Nias earthquake (solid grey, from *Meltzner et al.* [2015]), defining the Simeulue saddle. (b) History of interseismic vertical displacement at each coral site. The width of the bars is proportional to the vertical displacement rates. The dates of paleogeodetically recorded earthquakes are marked in red. The rate at PPY with a "+" sign (late in P3) indicates interseismic uplift. In this study, we model rate changes during periods P1, P2, and P3.

which span an ~1100 year long period from 870 to 2005 A.D. (Figure 1). This long paleogeodetic record reveals abrupt, sometimes coeval changes in long-term subsidence rates across the island. These observations implore the question: What tectonic mechanisms and physical processes control these rate variations?

In this study, we explain with physical models the observed rate changes during the past ~267 years—the time period spanning the past two seismic cycles (labeled periods P1, P2, and P3 in Figure 1). During this time, we find near-synchronous long-term rate changes above the northern limit of the 2005 M_w 8.6 Nias earthquake rupture patch. *Meltzner et al.* [2015] also examined the rate changes over this time period and presented simple models indicating that these observations can be explained as temporal changes in the width of the locked zone. In our study, we expand on those results with more sophisticated models and include data from additional coral sites located in the northwestern part of Simeulue. Our results suggest that the observed

interseismic rate changes can be explained by tectonically feasible spatiotemporal changes in interseismic coupling patterns.

2. Relative Sea Level Histories From Coral Microatolls

Relative sea level histories were derived from coral microatolls of the genera *Porites* and *Goniastrea* [*Meltzner et al.*, 2010, 2012, 2015]. The upper surfaces of these coral microatolls track relative sea level (RSL) changes over time.

Changes in RSL are a combined effect of both changes in land level and sea surface height, resulting from a combination of tectonic and nontectonic factors such as tectonic deformation over the earthquake cycle, isostatic changes of the land due to changing glacial and other surface loads, and regional changes in sea surface height due to oceanographic processes. It is therefore important to understand the relative contribution of these factors to RSL changes. As discussed by *Meltzner et al.* [2012], isostatic and oceanographic processes mostly operate on regional to global scales, and since Simeulue Island is only ~100 km long, these processes would be expected to influence all sites across the island approximately uniformly and synchronously. Although regional changes in sea surface height can result in spatially varying magnitudes of rate change at sites across the island, these variations are likely small in comparison to tectonic changes (further discussed in Text S1 in the supporting information). On the other hand, if rate changes observed on one part of the island are not observed coevally or coherently on another part of the island, then the spatial scale of these changes is more consistent with tectonic uplift and subsidence over the course of the earthquake cycle.

Such spatial variations in tectonic behavior are observed at Simeulue. For example, corals located over the 2004 M_w 9.2 Sumatra-Andaman earthquake rupture have distinctly different RSL histories from corals over the 2005 M_w 8.6 Nias earthquake rupture, suggesting that the central part of Simeulue acts as a persistent rupture barrier [*Meltzner et al.*, 2012]. Figure 1 illustrates the ~1100 year history of interseismic vertical displacement rate changes at 13 coral sites located on Simeulue. Table 1 lists the interseismic vertical displacement rates during each time period in the paleogeodetic record, for respective sites, as well as the 2σ uncertainties associated with each rate. During ~1300 to 1450 A.D., rate changes observed across the island are noncoeval. Most rate changes occur after major earthquakes, such as the 1394 A.D. earthquake, which affected sites over the 2004 patch [*Meltzner et al.*, 2010]. However, the paleogeodetic record also shows rate changes that are not associated with known earthquakes. For example, during ~1738 to 1861 A.D., sites over the 1861/2005 patch experienced a sudden acceleration in rates during the decades before the 1861 A.D. Nias-Simeulue earthquake. We discuss these rate changes in the next section, focusing on the ~267 year period from ~1738 to 2005 A.D.

3. Interseismic Vertical Displacement Rates During the Past ~267 Years

While it is relevant to investigate the entirety of this ~1100 year long record, in this study we focus on a particularly interesting period of interseismic rate changes observed during the ~267 year period from ~1738 to 2005 A.D. (P1, P2, and P3 in Figure 1). Above the 1861/2005 patch, four sites (SLR, SMB, UTG, and LBJ) experienced an abrupt four to tenfold acceleration in interseismic subsidence rates roughly 20–40 years prior to the 1861 earthquake (Figure 1). We note that corals in the Simeulue-Nias region show that the coseismic displacements of the 1861 Nias-Simeulue earthquake were similar to those of the 2005 Nias-Simeulue earthquake, suggesting that the two earthquakes were similar in extent and magnitude [*Meltzner et al.*, 2015]. These observations beg two questions: what patterns of strain accumulation and tectonic mechanisms explain the pre-1861 acceleration in rates? Were patterns and mechanisms of strain accumulation during the pre-2004 period (P3, Figure 1) similar to those preceding the 1861 earthquake? Modeling the interseismic vertical displacement rates during the last ~267 years will provide a better picture of the interseismic strain accumulation patterns over the past two seismic cycles on this section of the megathrust and of possible controlling tectonic mechanisms. We therefore develop physical models to explain three time periods in the past ~267 years: P1 (pre-1819), P2 (1839–1861), and P3 (pre-2004). We note that the start of the paleogeodetic record at individual coral sites differs for periods P1 and P3 (Table 1).

4. Modeling Methods

We develop physical models to understand the tectonic mechanisms controlling the rate variations during three time periods: P1, P2, and P3 (Figure 1). Our models consist of a fault with a dip profile that approximates

Table 1. Coral Site Locations and Interseismic Vertical Displacement Rates

Site	Longitude	Latitude	Time Period	Uplift Rate (mm/yr)[a]	Site Name (From *Meltzner et al.* [2010, 2012, 2015])	Notes
Langi	95.72130	2.82592	1961–1997 A.D.	−0.1 ± 2.2	LNG-A	
LNG			1962–1998 A.D.	−3.3 ± 2.2	LNG-A	
			1961–1998 A.D.	−1.7 ± 3.2	–	Weighted average[b]
Lewak	95.79091	2.92827	1301–1355 A.D.	−6.1 ± 1.5	LWK-B	
LWK			1397–1450 A.D.	−1.5 ± 1.5	LWK-B	
			1951–1997 A.D.	−3.3 ± 1.7	LWK-A	
			1962–1998 A.D.	−1.4 ± 2.2	LWK-A	
			1951–1998 A.D.	−2.6 ± 1.8	–	Weighted average[b]
Lhok Pauh	95.76324	2.86160	1346–1394 A.D.	−3.6 ± 1.7	LKP-B	
LKP			1409–1430 A.D.	−4.4 ± 3.8	LKP-B	
			1430–1450 A.D.	−3.5 ± 4.0	LKP-B	
			1945–1997 A.D.	−5.3 ±1.5	LKP-A	
			1962–1998 A.D.	−5.2 ± 2.2	LKP-A	
			1945–1998 A.D.	−5.3 ± 1.2	–	Weighted average[b]
Lhok Dalam	95.70072	2.74984	1327–1394 A.D.	−5.9 ± 1.2	LDL-B	
LDL			1982–1997 A.D.	−6.2 ± 5.3	LDL-A	
			1983–1998 A.D.	−8.7 ± 5.3	LDL-A	
			1982–1998 A.D.	−7.5 ± 3.8	–	Weighted average[b]
Ujung Sanggiran	95.86741	2.91213	1413–1450 A.D.	−7.2 ± 2.2	USG-A	
USG			1958–1997 A.D.	−2.2 ± 2.1	USG-A	
			1962–1998 A.D.	−2.2 ± 2.2	USG-A	
			1958–1998 A.D.	−2.2 ± 1.5	–	Weighted average[b]
Ujung Salang	95.75935	2.70612	886–956 A.D.	−4.7 ± 1.1	USL-A	
USL			1961–1997 A.D.	−7.6 ± 2.2	USL-A	
			1962–1998 A.D.	−7.1 ± 2.2	USL-A	
			1961–1998 A.D.	−7.4 ± 1.6	–	Weighted average[b]
Pulau Penyu	95.94407	2.85309	1449–1488 A.D.	−1.6 ± 2.1	PPY-A	
PPY			1488–1537 A.D.	−1.2 ± 1.6	PPY-A	
			1537–1565 A.D.	−5.6 ± 2.9	PPY-A	
			1928–1980 A.D.	−3.9 ± 1.5	PPY-A	
			1980–2002 A.D.	+0.3 ± 3.6	PPY-A	
Ujung Lambajo	95.99508	2.56620	1961–1997 A.D.	−7.4 ± 2.2	ULB-A	
ULB						
Silinggar	96.14749	2.70812	1800–1849 A.D.	−0.9 ± 1.6	SLR-A	
SLR			1849–1861 A.D.	−4.8 ± 6.7	SLR-A	
			1961–1997 A.D.	−4.2 ± 2.2	SLR-A	
Sambay	96.19470	2.65109	1760–1819 A.D.	−0.8 ± 1.4	SMB-A	
SMB			1819–1861 A.D.	−8.7 ±1.9	SMB-A	
Bunon	96.14427	2.51291	871–1024 A.D.	−0.5 ± 0.5	BUN-A	
BUN			1311–1340 A.D.	−2.2 ± 2.8	BUN-A	
			1353–1422 A.D.	−6.6 ± 1.2	BUN-A	
			1433–1466 A.D.	−0.3 ± 2.4	BUN-A	
			1481–1516 A.D.	−5.8 ± 2.3	BUN-A	
			1516–1538 A.D.	−10.1 ± 3.6	BUN-A	
			1545–1576 A.D.	−5.6 ± 2.6	BUN-A	
			1481–1576 A.D.	−6.0 ± 0.8	BUN-A	Average rate
			1982–1997 A.D.	−5.3 ± 5.3	BUN-A	
			1982–1997 A.D.	−8.9 ± 5.3	BUN-B	
			1982–1997 A.D.	−7.1 ± 3.8	–	Weighted average[b]

Table 1. (continued)

Site	Longitude	Latitude	Time Period	Uplift Rate (mm/yr)[a]	Site Name (From *Meltzner et al.* [2010, 2012, 2015])	Notes
Ujung Tinggi	96.27640	2.57304	1757–1839 A.D.	-1.1 ± 1.0	UTG-A	
UTG			1839–1861 A.D.	-7.0 ± 3.6	UTG-A	
			1982–1997 A.D.	-4.2 ± 5.3	UTG-A	
Labuhan Bajau	96.48623	2.40321	1738–1838 A.D.	-1.6 ± 0.8	LBJ-A	
LBJ			1838–1861 A.D.	-6.1 ± 3.5	LBJ-A	
			1945–1997 A.D.	-8.2 ± 1.5	LBJ-A	

[a]The 2σ total uncertainty equals the 2σ level of uncertainties due to differential coral erosion and growth rates (calculated with the methodology of *Meltzner et al.* [2012]).

[b]For period P3, two independent estimates of the pre-2004 rate were reported at seven coral sites: LNG, LWK, LKP, LDL, USG, USL, and BUN. For each of these sites, we calculated a weighted mean rate (WMR) (discussed in Text S1).

the Slab 1.0 model along this section of the megathrust [*Hayes et al.*, 2012] and extends to a depth of 100 km (Figure S2). The fault was divided into 5 km long and 2 km wide subfault patches.

We forward modeled the observed rate changes as spatiotemporal variations in locking depth and fault coupling. For each combination of fault parameters, the vertical displacement at each coral site was calculated with the Okada model of dislocations in an elastic half-space [*Okada*, 1985], in a backslip framework [*Savage*, 1983]. In this framework, slip on the fault can vary from zero to the full plate subduction rate. A slip rate of zero corresponds to a locked fault interface (with a coupling ratio of 1), whereas a slip rate equal to the full plate subduction rate corresponds to a freely slipping fault interface (with a coupling ratio of 0). In this study, we assumed that the plate subduction rate is 40 mm/yr [*McNeill and Henstock*, 2014; *Simons et al.*, 2007].

Our model configuration is similar to that employed by *Meltzner et al.* [2015]. In their study, they produced along-strike vertical displacement profiles based on a hypothetical row of surface points located equidistant from the trench. In this study, we incorporated sites in the northwestern part of Simeulue (for period P3), which are located at varying distances from the trench. We therefore calculated vertical displacement rates at each site based on their actual geographical locations.

It is believed that the frictional behavior of trench regions may be different from that at deeper seismogenic depths, and this is supported by observations of rapid afterslip that occurred updip of the 2005 rupture area [*Hsu et al.*, 2006]. Further, *Tilmann et al.* [2010] relocated aftershocks of the 2004 and 2005 earthquakes, and they found a well-defined updip limit of seismicity that lies at a fairly uniform distance from the trench, with the exception of an abrupt ~25 km landward shift under the central part of Simeulue. They inferred that this updip limit of seismicity marks the transition between the deeper seismogenic zone and stable sliding near the trench. In order to match these observations of the updip limit of seismicity, we followed the rationale outlined by *Meltzner et al.* [2015], assigning the shallowest 18 km of the fault to be partially coupled at a coupling ratio of 0.4 (Figure S2). We note that model resolution is poor in regions near the trench, and there will inevitably be tradeoffs between the parameters that characterize the coupling distribution in this region. Also, recent shallow, tsunamigenic megathrust ruptures along the Sumatran subduction zone [e.g., *Hill et al.*, 2012] suggest that the trench region is capable of both aseismic and seismic slip behavior.

For all three periods, we tested for along-strike variations by subdividing the fault into two sections and determined best fit combinations of (a) locking depths for each section and (b) the location of the boundary separating the two sections of different locking depths (Figure S2 shows an example model configuration). We systematically tested for downdip limits of locking ranging from 25 to 55 km depth, at 5 km (or in some cases finer) intervals (further details are described in Text S2). The preferred two section forward models for each time period correspond to the combinations of parameters that yield the least misfit between the data and model vertical displacement rates, based on the weighted mean of the sum of squared residuals (WMSSR). The WMSSR value is similar to the reduced chi-square value but uses the number of observations rather than the number of degrees of freedom in the model.

For periods P1 and P2, we have only three sites located in the southeastern part of the island, and hence, the data do not enable us to determine a well-resolved inverse model of fault coupling under the length of the island. We therefore chose to present for these periods a suite of possible forward models that can explain

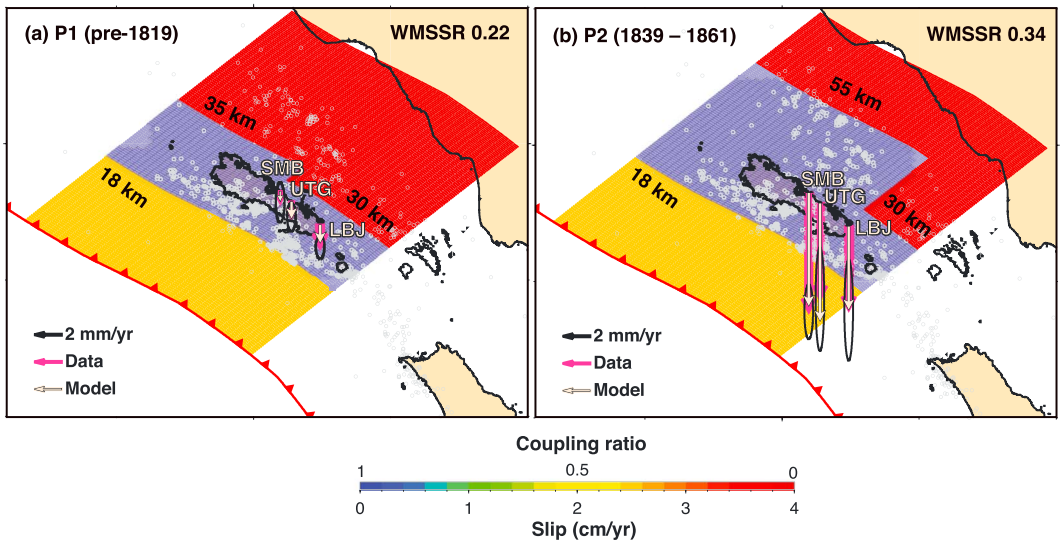

Figure 2. Preferred models of fault coupling for periods (a) P1 and (b) P2. The fourfold to tenfold acceleration in interseismic subsidence rates from period P1 to P2 can be explained by a deepening of the downdip limit of locking from 35 to 55 km under Simeulue. Grey circles: Seismicity from *Tilmann et al.* [2010].

the data (Figures S3–S7 and Tables S2–S4). In contrast, for period P3, additional coral observations from the northwestern part of Simeulue are available, which provide better model resolution under the length of the island. We therefore present for this period both forward and inverse models of fault coupling. For the forward models, we present the two section models described in the previous paragraph. In addition, we tested more complex forward models by incorporating a priori constraints based on observations of regional seismicity at Simeulue (more details in Text S3).

For the inverse models, we first designed a fault with the same dip geometry and size as employed for the forward models, but subdivided the fault into 10 by 10 km subfault patches. Similar to the forward models, we calculated model displacements at each site using Green's functions from *Okada* [1985]. We inverted for the slip rate deficit on each subpatch with a bounds-constrained linear least squares inversion method, assuming trench normal backslip on the fault. To regularize the inversion, we applied smoothing constraints and selected a Laplacian weight that yields a visually smooth spatial distribution of coupling (see Figure S8 and Text S4). The slip rate deficit is equal to some proportion of the full subduction rate of 40 mm/yr, such that the coupling ratio on each patch equals the slip rate deficit divided by the full subduction rate. We applied bounds of 0 mm/yr and 40 mm/yr to the slip rate deficit.

Due to the limited spatial distribution of data, we again emphasize that our models are limited in resolution and therefore nonunique. In particular, tradeoffs exist between the width of the locked zone and coupling ratio of the fault. Hence, even though we present a preferred model for each time period, many other models can explain the coral data within their uncertainties, and our models do not represent fully optimized solutions. Our goal in this study was simply to determine whether tectonically feasible models of spatially variable locking depths and fault coupling can explain the coral observations showing changing vertical displacement rates for each time period.

5. Results

Figure 2 shows our preferred forward models of spatially variable fault coupling for periods P1 and P2, and Figure 3 shows our preferred forward model and inverted coupling distribution for period P3. For period P1, our preferred model in Figure 2a has the fault locked to 35 km depth under northwestern Simeulue, while under southeastern Simeulue it is locked to 30 km depth (additional models in Figure S3). For period P2 (pre-1861), the fourfold to tenfold acceleration of interseismic subsidence rates can be explained by a deepening of the downdip limit of locking to 55 km under the entire length of Simeulue, with the fault remaining locked to 30 km depth southeast of Simeulue (Figure 2b; additional models in Figure S4). The downdip limit of locking changes from 55 to 30 km near the southeasternmost tip of Simeulue.

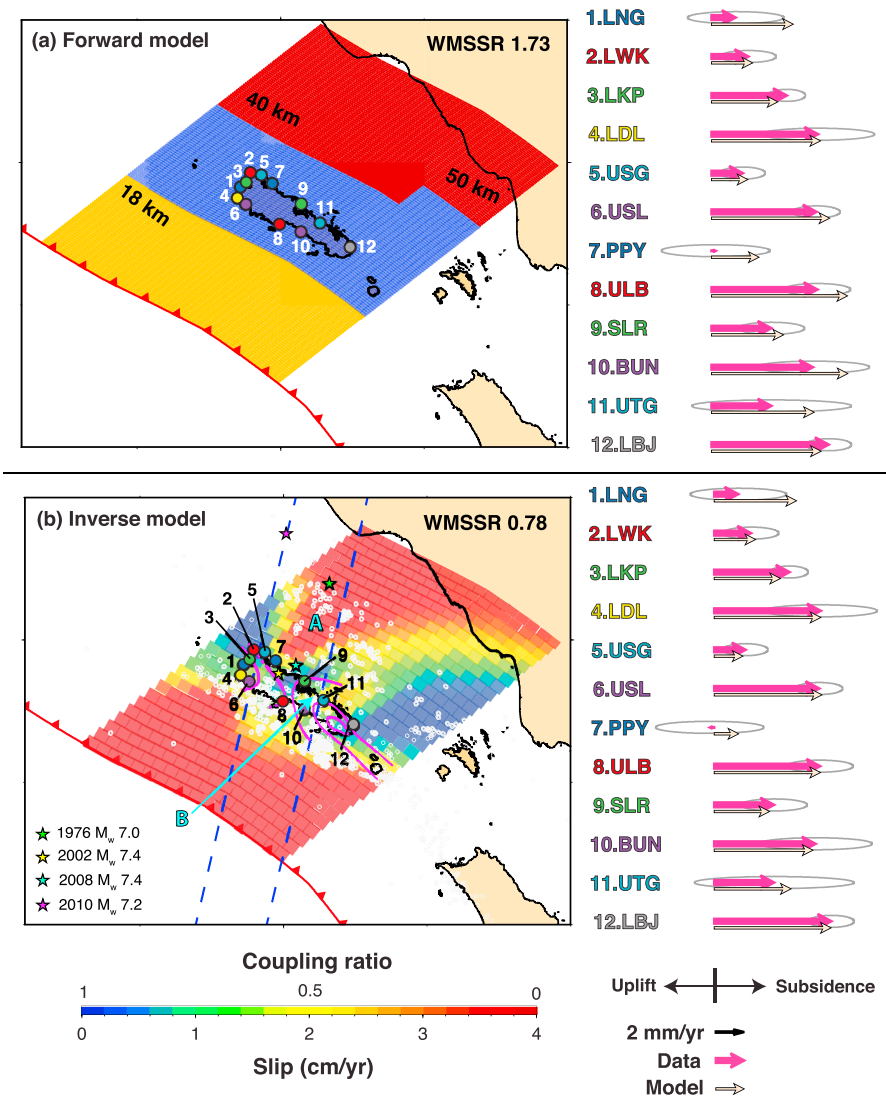

Figure 3. Preferred models of fault coupling for period P3. (a) Our preferred two-section forward model suggests that the fault was locked to a 40 km depth under Simeulue and 50 km under the southeasternmost part of the fault. (b) Our inverse model suggests that allowing for greater along-strike variations in locking depth and coupling under Simeulue yields better data – model fits. Four features observed in central Simeulue are overlain on the model: (1) The segment boundary location proposed by *Franke et al.* [2008] (blue dashed lines), (2) contours of coseismic uplift during the 2004 and 2005 earthquakes [*Meltzner et al.*, 2012, 2015] (dashed and solid magenta lines, respectively), (3) updip limit of seismicity [*Tilmann et al.*, 2010] (white circles), and (4) locations of four M ~ 7 earthquakes (stars from the Advanced National Seismic System (ANSS) catalog). Regions marked "A" and "B" are discussed in the text.

Our preferred two-section forward model for period P3 is shown in Figure 3a, which suggests that the fault was locked to 40 km depth under Simeulue, and 50 km under the southeasternmost part of the fault. The 10 km along-strike change in locking depth across the fault yields marginally better fits than a uniform locking depth of 40 km (Table S4a). Testing over a range of depths (results listed in Table S4a) suggests that a locking depth of 40 km under Simeulue yields the best data – model fits: neither shallower (35 km) nor deeper (50 km) downdip limits of locking yield good fits to the coral observations.

Our inverse model, shown in Figure 3b, shows that allowing for greater along-strike variations in fault coupling improves data – model fits, particularly at sites in the central part of Simeulue — USL, PPY, ULB, SLR, BUN, and UTG. This model suggests that the northwesternmost part of the fault was locked to ~40 km depth, while the southeasternmost part of the fault was locked to ~60 km. These locking depths are similar to those suggested

by our two-section forward model (Figure 3a). In contrast, marked variations in locking depth and coupling occur under Simeulue. Under the portion of northwestern Simeulue (marked A in Figure 3b) the fault is locked to a shallower depth of ~28–30 km. Also, the region under central-southern Simeulue (marked B in Figure 3b) is generally less coupled than adjacent parts of the fault. Although the details of regions A and B in the inverse model (Figure 3b) may be beyond the limits of what we can resolve with available data, all the models for P3 show less coupling under central Simeulue, regardless of the patch size and Laplacian weight that we tested (Figure S8 and Text S4). This result suggests that lower coupling under central Simeulue in P3 is a robust conclusion. Moreover, we tested forward models with greater along-strike complexity (Text S3), and our results suggest that data – model fits indeed improve when shallower downdip limits of locking, deeper updip limits of full locking, and less fault coupling under central Simeulue are integrated into our models (Figure S6).

As noted in the previous section, our models are limited in resolution and hence nonunique. We therefore present various other possible models for each of the three time periods in Figures S3–S7 and Tables S2–S4 (Text S2 details a discussion of these figures and tradeoffs between various model parameters, among our two-section forward models). Our main conclusion from these models is that there exist tectonically feasible ranges of locking depths that can explain the coral observations for each time period. Based on this, we argue that the time-varying vertical displacement rates on Simeulue are likely tectonically controlled.

6. Discussion

Our suites of models suggest that for periods P2 and P3, the patterns of fault coupling were different (compare Figures 2b, 3a, and 3b). The differences in the models of fault coupling between the two periods may in part reflect the more limited spatial distribution of data across the island for period P2, but different vertical displacement rates (although not significant at 2σ) at sites with rates estimated before each earthquake suggest that patterns of strain accumulation in the decades before the 1861 and 2005 earthquakes may have been different.

The along-strike variations in locking depths and fault coupling suggested by our inverse model for period P3 may be a manifestation of the persistent rupture barrier in central Simeulue. This barrier is characterized by low cumulative slip during the 2004 and 2005 ruptures and localized M7+ earthquakes in 1976, 2002, 2008, and 2010 (Figure 3b). In addition, *Meltzner et al.* [2012] showed that at least seven large ruptures were arrested at this barrier over the past ~1100 years. Researchers have previously associated this barrier with structural heterogeneities on the subducting plate and different frictional properties on the fault interface. Notably, *Franke et al.* [2008] conducted wide angle refraction and multichannel reflection seismic surveys along this part of the megathrust, and their results reveal an elevated NNE-SSW oriented ridge of oceanic basement under central Simeulue, which projects to the location of one of the main fracture zones in the Wharton basin, as mapped by *Singh et al.* [2011] and *Jacob et al.* [2014]. They interpret this ridge to reflect the structural relief caused by a fracture zone on the subducting plate at central Simeulue. The orientation of this ridge is consistent with the orientation of the Simeulue saddle in the middle of the island, as defined by contours of uplift from the coseismic rupture ends of the 2004 and 2005 earthquakes [*Briggs et al.*, 2006; *Meltzner et al.*, 2015].

Figure 3b shows an overlay of the proposed location of the aforementioned features onto our coupling model. A visual comparison shows that the shallower downdip limit of locking under northwestern Simeulue (marked A in Figure 3b) lies in the region of the proposed location of the subducted fracture zone. The region of lower coupling that is marked B in Figure 3b coincides spatially with the eastern flank of the subducted fracture zone, where *Franke et al.* [2008] proposed that the megathrust is faulted and torn. The eastern flank is also marked by a ~25 km landward shift in the updip limit of seismicity, a feature that may reflect the structural heterogeneities in this region. We speculate that the lower apparent coupling in region B may be attributed to a fault or tear in the megathrust at this location.

The time-varying interseismic rates suggest that interseismic fault coupling and slip behavior may be influenced by frictional conditions along the fault that can change with time. Localized fluid release from the subducted fracture zone, as proposed by *Tilmann et al.* [2010], might lead to transient changes in pore pressure on the fault interface. This increased fluid pressure in turn reduces the effective normal stress and changes the frictional properties on the megathrust, since fault friction is controlled by factors such as normal stress, temperature, type of rock material, and distribution of fluids in the crust [*Kaneko et al.*, 2010].

Numerical simulations of the seismic cycle will enable us to gain further insights into how these factors control friction and interseismic behavior of faults. For example, *Noda and Hori* [2014] conducted simulations of a sequence of earthquakes assuming a rate and state friction law and reported that the A/B parameter (direct effect/evolution effect) controls the complexity of interseismic behavior on seismogenic patches. Until now, it remains poorly understood how tectonic and physical processes vary over multiple seismic cycles at subduction zones and justifies the need to combine observations of multicycle geodetic records with modeling efforts in order to obtain a holistic picture of the physical factors that control time-varying interseismic behavior of megathrusts.

7. Conclusion

Coral microatolls on Simeulue Island reveal vertical displacement rates that vary with time over the past ~1100 years. Our results suggest that these rate variations are likely tectonically controlled and that the strain accumulation process is not uniform during the interseismic period of the seismic cycle. In the decades prior to the 1861 Simeulue-Nias earthquake, coral observations reveal a fourfold to tenfold acceleration in interseismic subsidence rates. One way to explain these observations is with a significant deepening of the downdip limits of locking under the island. In addition, despite similar coseismic rupture areas of the 1861 and 2005 earthquakes, the pattern of interseismic fault coupling in the decades prior to the two earthquakes may have been different. Up to now, multicycle geodetic records at subduction zones are sparse, but obtaining such records is essential to improve our understanding of how interseismic behavior on megathrusts varies with time.

Acknowledgments

This research was supported by the National Research Foundation Singapore under its Singapore NRF Fellowship scheme (NRF Award NRF-NRFF2010-064), by the Earth Observatory of Singapore (EOS), by the Singapore Ministry of Education (MOE) under the Research Centers of Excellence initiative, and by a Nanyang Technological University Startup Grant. L.Tsang was supported by a Singapore International Graduate Award and an EOS research scholarship. J. Freymueller was supported by NSF grant EAR-1215933. This work comprises Earth Observatory of Singapore contribution number 107. We express our thanks to B. Suwargadi, D. Natawidjaja, D. Prayudi, I. Suprihanto, R. Briggs, B. Philibosian, and J. Galetzka for their field support. We are grateful for linguistic advice from P. Adamek which significantly improved the structure of this paper. We thank Q. Qiu, S. Barbot, and L. Feng for their insightful discussions. We express our thanks to the Editor, Andrew Newman, and Roland Bürgmann for their detailed and constructive comments that have greatly improved this paper. Earthquake locations from the Advanced National Seismic System (ANSS) catalog were accessed through the Northern California Earthquake Data Center (NCEDC), doi:10.7932/NCEDC.

References

Briggs, R., et al. (2006), Deformation and slip along the Sunda megathrust in the great 2005 Nias-Simeulue earthquake, *Science*, *311*(5769), 1897–1901.

Chlieh, M., J.-P. Avouac, K. Sieh, D. H. Natawidjaja, and J. Galetzka (2008), Heterogeneous coupling of the Sumatran megathrust constrained by geodetic and paleogeodetic measurements, *J. Geophys. Res.*, *113*, B05305, doi:10.1029/2007JB004981.

Franke, D., M. Schnabel, S. Ladage, D. R. Tappin, S. Neben, Y. S. Djajadihardja, C. Müller, H. Kopp, and C. Gaedicke (2008), The great Sumatra-Andaman earthquakes-imaging the boundary between the ruptures of the great 2004 and 2005 earthquakes, *Earth Planet. Sci. Lett.*, *269*(1), 118–130.

Freymueller, J. T., S. C. Cohen, and H. J. Fletcher (2000), Spatial variations in present-day deformation, Kenai Peninsula, Alaska, and their implications, *J. Geophys. Res.*, *105*(B4), 8079–8101.

Fu, Y., and J. T. Freymueller (2013), Repeated large slow slip events at the southcentral Alaska subduction zone, *Earth Planet. Sci. Lett.*, *375*, 303–311.

Hayes, G. P., D. J. Wald, and R. L. Johnson (2012), Slab1.0: A three-dimensional model of global subduction zone geometries, *J. Geophys. Res.*, *117*, B01302, doi:10.1029/2011JB008524.

Hill, E., et al. (2012), The 2010 M_w 7.8 Mentawai earthquake: Very shallow source of a rare tsunami earthquake determined from tsunami field survey and near-field GPS data, *J. Geophys. Res.*, *117*, B06402, doi:10.1029/2012JB009159.

Hsu, Y.-J., M. Simons, J.-P. Avouac, J. Galetzka, K. Sieh, M. Chlieh, D. Natawidjaja, L. Prawirodirdjo, and Y. Bock (2006), Frictional afterslip following the 2005 Nias-Simeulue earthquake, Sumatra, *Science*, *312*(5782), 1921–1926.

Jacob, J., J. Dyment, and V. Yatheesh (2014), Revisiting the structure, age, and evolution of the Wharton Basin to better understand subduction under Indonesia, *J. Geophys. Res. Solid Earth*, *119*, 169–190, doi:10.1002/2013JB010285.

Kaneko, Y., J.-P. Avouac, and N. Lapusta (2010), Towards inferring earthquake patterns from geodetic observations of interseismic coupling, *Nat. Geosci.*, *3*(5), 363–369.

Li, S., J. T. Freymueller, and R. McCaffrey (2014), Time-dependent variations of slow slip events in Lower Cook Inlet of the Alaska-Aleutian subduction zone, Abstract #S53C-4511 presented at 2014 Fall Meeting, AGU, San Francisco, Calif., 14–18 Dec.

Lorito, S., F. Romano, S. Atzori, X. Tong, A. Avallone, J. McCloskey, M. Cocco, E. Boschi, and A. Piatanesi (2011), Limited overlap between the seismic gap and coseismic slip of the great 2010 Chile earthquake, *Nat. Geosci.*, *4*(3), 173–177.

Loveless, J. P., and B. J. Meade (2011), Spatial correlation of interseismic coupling and coseismic rupture extent of the 2011 M_w = 9.0 Tohoku-oki earthquake, *Geophys. Res. Lett.*, *38*, L17306, doi:10.1029/2011GL048561.

McNeill, L. C., and T. J. Henstock (2014), Forearc structure and morphology along the Sumatra-Andaman subduction zone, *Tectonics*, *33*, 112–134, doi:10.1002/2012TC003264.

Meade, B. J., and J. P. Loveless (2009), Predicting the geodetic signature of $M_w >= 8$ slow slip events, *Geophys. Res. Lett.*, *36*, L01306, doi:10.1029/2008GL036364.

Meltzner, A. J., K. Sieh, H.-W. Chiang, C.-C. Shen, B. W. Suwargadi, D. H. Natawidjaja, B. E. Philibosian, R. W. Briggs, and J. Galetzka (2010), Coral evidence for earthquake recurrence and an A.D. 1390–1455 cluster at the south end of the 2004 Aceh-Andaman rupture, *J. Geophys. Res.*, *115*, B10402, doi:10.1029/2010JB007499.

Meltzner, A. J., K. Sieh, H.-W. Chiang, C.-C. Shen, B. W. Suwargadi, D. H. Natawidjaja, B. Philibosian, and R. W. Briggs (2012), Persistent termini of 2004- and 2005-like ruptures of the Sunda megathrust, *J. Geophys. Res.*, *117*, B04405, doi:10.1029/2011JB008888.

Meltzner, A. J., K. Sieh, H.-W. Chiang, C.-C. Wu, L. L. H. Tsang, C.-C. Shen, E. M. Hill, B. W. Suwargadi, D. Natawidjaja, B. Philibosian, and R. W. Briggs (2015), Time-varying interseismic strain rates and similar seismic ruptures on the Nias-Simeulue patch of the Sunda megathrust, *Quart. Sci. Rev.*, *122*, 258–281, doi:10.1016/j.quascirev.2015.06.003.

Metois, M., A. Socquet, and C. Vigny (2012), Interseismic coupling, segmentation and mechanical behavior of the central Chile subduction zone, *J. Geophys. Res.*, *117*, B03406, doi:10.1029/2011JB008736.

Miura, S., Y. Suwa, A. Hasegawa, and T. Nishimura (2004), The 2003 M8.0 Tokachi-Oki earthquake—How much has the great event paid back slip debts?, *Geophys. Res. Lett.*, *31*, L05613, doi:10.1029/2003GL019021.

Moreno, M., M. Rosenau, and O. Oncken (2010), Maule earthquake slip correlates with pre-seismic locking of Andean subduction zone, *Nature*, *467*(7312), 198–202.

Moreno, M., et al. (2011), Heterogeneous plate locking in the South–Central Chile subduction zone: Building up the next great earthquake, *Earth Planet. Sci. Lett.*, *305*(3), 413–424.

Nalbant, S., J. McCloskey, S. Steacy, M. NicBhloscaidh, and S. Murphy (2013), Interseismic coupling, stress evolution, and earthquake slip on the Sunda megathrust, *Geophys. Res. Lett.*, *40*, 4204–4208, doi:10.1002/grl.50776.

Nishimura, T., T. Hirasawa, S. Miyazaki, T. Sagiya, T. Tada, S. Miura, and K. Tanaka (2004), Temporal change of interplate coupling in northeastern Japan during 1995–2002 estimated from continuous GPS observations, *Geophys. J. Int.*, *157*(2), 901–916.

Noda, H., and T. Hori (2014), Under what circumstances does a seismogenic patch produce aseismic transients in the later interseismic period?, *Geophys. Res. Lett.*, *41*, 7477–7484, doi:10.1002/2014GL061676.

Okada, Y. (1985), Surface deformation due to shear and tensile faults in a half-space, *Bull. Seismol. Soc. Am.*, *75*(4), 1135–1154.

Paul, J., C. Rajendran, A. Lowry, V. Andrade, and K. Rajendran (2012), Andaman postseismic deformation observations: Still slipping after all these years?, *Bull. Seismol. Soc. Am.*, *102*(1), 343–351.

Philibosian, B., K. Sieh, J.-P. Avouac, D. H. Natawidjaja, H.-W. Chiang, C.-C. Wu, H. Perfettini, C.-C. Shen, M. R. Daryono, and B. W. Suwargadi (2014), Rupture and variable coupling behavior of the Mentawai segment of the Sunda megathrust during the supercycle culmination of 1797 to 1833, *J. Geophys. Res. Solid Earth*, *119*, 7258–7287, doi:10.1002/2014JB011200.

Prawirodirdjo, L., R. McCaffrey, C. D. Chadwell, Y. Bock, and C. Subarya (2010), Geodetic observations of an earthquake cycle at the Sumatra subduction zone: Role of interseismic strain segmentation, *J. Geophys. Res.*, *115*, B03414, doi:10.1029/2008JB006139.

Romano, F., A. Piatanesi, S. Lorito, N. D'Agostino, K. Hirata, S. Atzori, Y. Yamazaki, and M. Cocco (2012), Clues from joint inversion of tsunami and geodetic data of the 2011 Tohoku-oki earthquake, *Sci. Rep.*, *2*, 385, doi:10.1038/srep00385.

Savage, J. (1983), A dislocation model of strain accumulation and release at a subduction zone, *J. Geophys. Res.*, *88*(B6), 4984–4996.

Simons, W., et al. (2007), A decade of GPS in southeast Asia: Resolving Sundaland motion and boundaries, *J. Geophys. Res.*, *112*, B06420, doi:10.1029/2005JB003868.

Singh, S. C., H. Carton, A. S. Chauhan, S. Androvandi, A. Davaille, J. Dyment, M. Cannat, and N. D. Hananto (2011), Extremely thin crust in the Indian Ocean possibly resulting from Plume–Ridge interaction, *Geophys. J. Int.*, *184*(1), 29–42.

Suito, H., and J. T. Freymueller (2009), A viscoelastic and afterslip postseismic deformation model for the 1964 Alaska earthquake, *J. Geophys. Res.*, *114*, B11404, doi:10.1029/2008JB005954.

Thirumalai, K., F. W. Taylor, C.-C. Shen, L. L. Lavier, C. Frohlich, L. M. Wallace, C.-C. Wu, H. Sun, and A. K. Papabatu (2015), Variable Holocene deformation above a shallow subduction zone extremely close to the trench, *Nat. Commun.*, *6*, 7607, doi:10.1038/ncomms8607.

Tilmann, F., T. Craig, I. Grevemeyer, B. Suwargadi, H. Kopp, and E. Flueh (2010), The updip seismic/aseismic transition of the Sumatra megathrust illuminated by aftershocks of the 2004 Aceh-Andaman and 2005 Nias events, *Geophys. J. Int.*, *181*(3), 1261–1274.

Tsang, L. L. H., A. J. Meltzner, B. Philibosian, E. M. Hill, J. T. Freymueller, and K. Sieh (2015), A 15-year slow slip event on the Sunda megathrust offshore Sumatra, *Geophys. Res. Lett.*, *42*, 6630–6638, doi:10.1002/2015GL064928.

Wesson, R., D. Melnick, M. Cisternas, M. Moreno, and L. L. Ely (2015), Vertical deformation through a complete seismic cycle at Isla Santa Maria, Chile, *Nat. Geosci.*, *8*, 547–551.